Bandgap lattices: low index solitons and linear properties

Nikolaos K. Efremidis and Kyriakos Hizanidis

School of Electrical and Computer Engineering, National Technical University of Athens, Athens 15773, Greece

efraim@central.ntua.gr, kyriakos@central.ntua.gr

Abstract: A new type of waveguide lattice that relies on the effect of bandgap guidance, rather than total internal reflection, in the regions between the waveguide defects is proposed. Two different setting, for low index and high index defects are suggested. We analyze the linear bandgap and diffraction properties of such lattices. In the nonlinear regime the Kerr effect can counteract diffraction leading to the formation of gap lattice solitons. Interestingly enough, in the case of low index defects, stable soliton solutions are localized in the low index areas. This finding challenges the widely accepted idea that stable solitons can be sustained in high refractive index regions. In addition, in the case of high index defects, the coupling coefficient can become negative. Physical settings where the linear and nonlinear properties for bandgap lattices can be experimentally realized are presented.

OCIS codes: (130.2790) Integrated optics.Guided waves; (190.5530) Nonlinear Optics.Pulse propagation and solitons; (999.9999) Photonic Lattices

References and links

1. E. Yablonovitch, "Inhibited Spontaneous Emission in Solid-State Physics and Electronics," Phys. Rev. Lett. **58**, 2059–2062 (1987).
2. S. John, "Strong Localization of Photons in Certain Disordered Dielectric Superlattices," Phys. Rev. Lett. **58**, 2486–2489 (1987).
3. J. Joannopoulos, R. Meade, and J. N. Winn, *Photonic Crystals: Molding the Flow of Light* (Princeton University Press, Princeton, NJ, 1995).
4. J. Knight, J. Broeng, T. A. Birks, and P. Russell, "Photonic band gap guidance in optical fibers," Science **282**, 1476–1478 (1998).
5. P. Russell, "Photonic crystal fibers," Science **299**, 358–362 (2003).
6. D. N. Christodoulides and R. I. Joseph, "Discrete self-focusing in nonlinear arrays of coupled waveguides," Opt. Lett. **13**, 794–796 (1988).
7. H. S. Eisenberg, Y. Silberberg, R. Morandotti, A. R. Boyd, and J. S. Aitchison, "Discrete Spatial Optical Solitons in Waveguide Arrays," Phys. Rev. Lett. **81**, 3383–3386 (1998).
8. D. N. Christodoulides, F. Lederer, and Y. Silberberg, "Discretizing light behaviour in linear and nonlinear waveguide lattices," Nature **424**, 817–823 (2003).
9. A. Mekis, J. C. Chen, I. Kurland, S. Fan, P. R. Villeneuve, and J. D. Joannopoulos, "High Transmission through Sharp Bends in Photonic Crystal Waveguides," Phys. Rev. Lett. **77**, 3787–3790 (1996).
10. S. L. McCall, P. M. Platzman, R. Dalichaouch, D. Smith, and S. Schultz, "Microwave Propagation in Two-Dimensional Dielectric Lattices," Phys. Rev. Lett. **67**, 2017–2020 (1991).
11. E. Yablonovitch, T. J. Gmitter, R. D. Meade, A. M. Rappe, K. D. Brommer, and J. D. Joannopoulos, "Donor and Acceptor Modes in Photonic Band Strucure," Phys. Rev. Lett. **67**, 3380–3383 (1991).
12. N. Stefanou and A. Modinos, "Impurity bands in photonic insulators," Phys. Rev. B **57**, 12,127–12,133 (1998).
13. A. Yariv, Y. Xu, R. K. Lee, and A. Scherer, "Coupled-resonator optical waveguide: a proposal and analysis," Opt. Lett. **24**, 711–713 (1999).

#9692 - $15.00 USD Received 22 November 2005; revised 6 December 2005; accepted 6 December 2005

14. M. Bayindir, B. Temelkuran, and E. Ozbay, "Tight-Binding Description of the Coupled Defect Modes in Three-Dimensional Photonic Crystals," Phys. Rev. Lett. **84**, 2140–2143 (2000).
15. R. Morandotti, U. Peschel, J. S. Aitchison, H. S. Eisenberg, and Y. Silberberg, "Dynamics of Discrete Solitons in Optical Waveguide Arrays," Phys. Rev. Lett. (1999).
16. R. Iwanow, R. Schiek, G. I. Stegeman, T. Pertsch, F. ederer, Y. Min, and W. Sohler, "Observation of Discrete Quadratic Solitons," Phys. Rev. Lett. **93**, 113,902–1–4 (2004).
17. T. Pertsch, P. Dannberg, W. Elflein, A. Bräuer, and F. Lederer, "Optical Bloch Oscillations in Temperature Tuned Waveguide Arrays," Phys. Rev. Lett. **83**, 4752–4755 (1999).
18. R. Morandotti, U. Peschel, J. S. Aitchison, H. S. Eisenberg, and Y. Silberberg, "Experimental Observation of Linear and Nonlinear Optical Bloch Oscillations," Phys. Rev. Lett. **83**, 4756–4759 (1999).
19. J. Meier, J. Hudock, D. Christodoulides, G. Stegeman, Y. Silberberg, R. Morandotti, and J. S. Aitchison, "Discrete Vector Solitons in Kerr Nonlinear Waveguide Arrays," Phys. Rev. Lett. **91**, 143,907–1–4 (2003).
20. D. Mandelik, H. S. Eisenberg, Y. Silberberg, R. Morandotti, and J. S. Aitchison, "Band-Gap Structure ofWaveguide Arrays and Excitation of Floquet-Bloch Solitons," Phys. Rev. Lett. **90**, 053,902–1–4 (2003).
21. J. W. Fleischer, T. Carmon, M. Segev, N. K. Efremidis, and D. N. Christodoulides, "Observation of discrete solitons in optically-induced real-time waveguide arrays," Phys. Rev. Lett. **90**, 023,902–1–4 (2003).
22. J. Feng, "Alternative scheme for studying gap solitons in an infinite periodic Kerr medium," Opt. Lett. **18**, 1302–1304 (1993).
23. D. D. Mandelik, R. Morandotti, J. S. Aitchison, and Y. Silberberg, "Gap Solitons inWaveguide Arrays," Phys. Rev. Lett. **92**, 093,904–1–4 (2004).
24. D. Neshev, A. A. Sukhorukov, B. Hanna, W. Krolikowski, and Y. S. Kivshar, "Controlled Generation and Steering of Spatial Gap Solitons," Phys. Rev. Lett. **93**, 083,905–1–4 (2004).
25. P. J. Y. Louis, E. A. Ostrovskaya, C. M. Savage, and Y. S. Kivshar, "Bose-Einstein condensates in optical lattices: Band-gap structure and solitons," Phys. Rev. A **67**, 013,602–1–9 (2003).
26. N. K. Efremidis and D. N. Christodoulides, "Lattice solitons in Bose-Einstein condensates," Phys. Rev. A **67**, 063,608–1–9 (2003).
27. Y. V. Kartashov, V. A. Vysloukh, and L. Torner, "Soliton trains in photonic lattices," Opt. Express **12**, 2831–2837 (2004).
28. J. Wang, F. Ye, L. Dong, T. Cai, and Y.-P. Li, "Lattice solitons supported by competing cubic-quintic nonlinearity," Phys. Lett. A **339**, 74–82 (2005).
29. P. Kevrekidis, B. Malomed, and Z. Musslimani, "Discrete gap solitons in a diffraction-managed waveguide array," Eur. Phys. J. D **23**, 421–436 (2003).
30. D. N. Christodoulides and R. I. Joseph, "Slow Bragg Solitons in Nonlinear Periodic Structures," Phys. Rev. Lett. **62**, 1746–1749 (1989).
31. A. B. Aceves and S. Wabnitz, "Self-induced transparency solitons in nonlinear refractive periodic media," Phys. Lett. A **141**, 37–42 (1989).
32. B. J. Eggleton, R. E. Slusher, C. M. de Sterke, P. A. Krug, and J. E. Sipe, "Bragg Grating Solitons," Phys. Rev. Lett. **76**, 1627–1630 (1996).
33. C. M. de Sterke and J. E. Sipe, "Gap solitons," in *Progress in Optics*, E. Wolf, ed., vol. XXXIII, p. 203 (North-Holland, Amsterdam, 1994).
34. F. Fedele, J. Yang, and Z. Chen, "Defect modes in one-dimensional photonic lattices," Opt. Lett. **30**, 1506–1508 (2005).
35. Y. V. Kartashov, L. Torner, and V. A. Vysloukh, "Diffraction management of focused light beams in optical lattices with a quadratic frequency modulation," Opt. Express **13**, 4244–4249 (2005).
36. N. K. Efremidis, D. N. Christodoulides, S. Sears, J. W. Fleischer, and M. Segev, "Discrete Solitons in Photorefractive Optically-Induced Photonic Lattices," Phys. Rev. E **66**, 046,602–1–5 (2002).
37. J. W. Fleischer, M. Segev, N. K. Efremidis, and D. N. Christodoulides, "Observation of two-dimensional discrete solitons in optically-induced nonlinear photonic lattices," Nature **422**, 147–150 (2003).
38. N. K. Efremidis, J. Hudock, D. N. Christodoulides, J. W. Fleischer, O. Cohen, and M. Segev, "Two-dimensional optical lattice solitons," Phys. Rev. Lett. **91**, 213,906–1–4 (2003).
39. J. Yang and Z. H. Musslimani, "Fundamental and vortex solitons in a two-dimensional optical lattice," Opt. Lett. **21**, 2094–2096 (2003).
40. B. A. Malomed and P. G. Kevrekidis, "Discrete vortex solitons," Prys. Rev. E **64**, 026,601–1–6 (2001).
41. B. B. Baizakov, B. A. Malomed, and M. Salerno, "Multidimensional solitons in periodic potentials," Europhys. Lett. **63**, 642–648 (2003).
42. J. W. Fleischer, G. Bartal, O. Cohen, O. Manela, M. Segev, J. Hudock, and D. N. Christodoulides, "Observation of Vortex-Ring "Discrete" Solitons in 2D Photonic Lattices," Phys. Rev. Lett. **92**, 123,904–1–4 (2004).
43. D. N. Neshev, T. J. Alexander, E. A. Ostrovskaya, Y. S. Kivshar, H. Martin, I. Makasyuk, and Z. Chen, "Observation of Discrete Vortex Solitons in Optically Induced Photonic Lattices," Phys. Rev. Lett. **92**, 123,903–1–4 (2004).
44. Y. V. Kartashov, V. A. Vysloukh, and L. Torner, "Rotary Solitons in Bessel Optical Lattices," Phys. Rev. Lett. **93**, 093,904–1–4 (2004).

#9692 - $15.00 USD Received 22 November 2005; revised 6 December 2005; accepted 6 December 2005

45. Y. V. Kartashov, A. A. Egorov, L. Torner, and D. N. Christodoulides, "Stable soliton complexes in two-dimensional photonic lattices," Opt. Lett. **29**, 1918–1920 (2004).
46. J. W. Fleischer, G. Bartal, O. Cohen, T. Schwartz, O. Manela, B. Freeman, M. Segev, H. Buljan, and N. K. Efremidis, "Spatial photonics in nonlinear waveguide arrays," Opt. Express **13**, 1780–1796 (2005).
47. P. Yeh and A. Yariv, "Bragg reflection waveguides," Opt. Commun. **19**, 427–430 (1976).
48. A. Y. Cho, A. Yariv, and P. Yeh, "Observation of confined propagation in Bragg waveguides," Appl. Phys. Lett. **30**, 471 (1977).
49. A. Yariv, "Coupled-wave formalism for optical waveguiding by transverse Bragg reflection," Opt. Lett. **27**, 936–938 (2002).
50. S. Linden, J. P. Mondia, H. M. V. Driel, T. C. Kleckner, C. R. Stanley, D. Modotto, A. Locatelli, C. D. Angelis, R. Morandotti, and J. S. Aitchison, "Nonlinear transmission properties of a deep-etched microstructured waveguide," Appl. Phys. Lett. **84**, 5437–5439 (2004).
51. H. Martin, E. D. Eugenieva, Z. Chen, and D. N. Christodoulides, "Discrete Solitons and Soliton-Induced Dislocations in Partially Coherent Photonic Lattices," Phys. Rev. Lett. **92**, 123,902–1–4 (2004).
52. T. M. Monro, D. J. Richardson, N. G. R. Broderick, and P. J. Bennett, "Holey Optical Fibers: An Efficient Modal Model," J. Lightwave Technol. **17**, 1093–1102 (1999).
53. R. d. L. Kronig and W. G. Penney, "Quantum Mechanics of Electrons in Crystal Lattices," P. Roy. Soc. Lond. A Mat. **814**, 499–513 (1931).
54. S. Theodorakis and E. Leontidis, "Bound states in a nonlinear Kronig-Penney model," J. Phys. A **30**, 4835–4849 (1997).
55. W. Li and A. Smerzi, "Nonlinear Krönig-Penney model," Phys. Rev. E **70**, 016,605–1–4 (2004).
56. I. M. Merhasin, B. V. Gisin, R. Driben, and B. A. Malomed, "Finite-band solitons in the Kronig-Penney model with the cubic-quintic nonlinearity," Phys. Rev. E **71**, 016,613–1–12 (2005).
57. C. Kittel, *Introduction to Solid State Physics* (Wiley, New York, 1986).
58. H. S. Eisenberg, Y. Silberberg, R. Morandotti, and J. S. Aitchison, "Diffraction Management," Phys. Rev. Lett. **85**, 1863–1866 (2000).
59. S. F. Mingaleev and R. A. Kivshar, Yuri S.and Sammut, "Long-range interaction and nonlinear localized modes in photonic crystal waveguides," Phys. Rev. E **62**, 5777–5782 (2000).
60. J. Sipe and H. G. Winful, "Nonlinear Schrödinger solitons in a periodic structure," Opt. Lett. **13**, 132–133 (1988).

1. Introduction

The field of linear and nonlinear dynamics in periodic optical systems recently attracts considerable attention. Periodic and random refractive index modulations have been studied in the context of photonic crystals [1–3], Photonic Crystal Fibers (PCFs) [4, 5], and optical lattices [6–8]. The motivation for these studies is twofold: to understand fundamental physical properties of optical field propagation in periodic media and to develop tomorrow's optical switching devices.

It is known that in photonic crystals the behavior of photons can be significantly altered in two and three-dimensional periodic [1] and random [2] optical media. As a result, artificially microstructured materials with specific crystal structures and index contrasts can exhibit complete two or three dimensional photonic bandgaps at some range of frequencies. An optical bandgap is an effective way to control photons compared to traditional waveguiding that relies on the effect of Total Internal Reflection (TIR). For example, transmission of light thought sharp corners in photonic bandgap waveguides is much more efficient as compared to TIR waveguides [9]. If an inhomogeneity or defect is introduced in the lattice with a complete bandgap, localized electromagnetic modes oscillating with frequencies within the bandgap can occur [10, 11]. A PCF can be considered as a different type of two-dimensional defect, guiding light over long distances. Furthermore, a periodic sequence of microcavities embedded in a PC has recently been proposed [12–14]. In such a system waveguiding is accomplished via light hopping or tunneling among successive microcavities.

On the other hand, recent theoretical and experimental progress in the field of linear and nonlinear dynamics in optical lattices has been motivated by the success of early stage experiments in this area [7, 15]. The simplest type of one-dimensional optical lattice is a sequence (array) of waveguides [6, 8]. In this model, energy can couple between adjacent waveguides though

#9692 - $15.00 USD Received 22 November 2005; revised 6 December 2005; accepted 6 December 2005

evanescent wave TIR coupling. Optical waveguides have provided a fertile ground to study one-dimensional linear and nonlinear optical wave dynamics in periodic systems. These include the prediction and experimental observation of solitons in Kerr [6, 7] and quadratic media [16], Bloch oscillations [17, 18], discrete vector solitons [19], and the study of the bandgap structure of linear and nonlinear waves [20]. Gap solitons were experimentally observed in [20, 21] and it was shown that using a two-beam interference method, suggested in [22], can provide a better excitation for gap solitons [23, 24]. Theoretical works about solitons in deep periodic lattices include the study of fundamental and higher order gap solitons in self-focusing and self-defocusing media [25, 26] as well as twisted modes and complexes [27], solitons in cubic/quintic media [28], and in linearly/nonlinearly coupled waveguide arrays [29]. Gap solitons were first studied in the context of optical fibers using coupled mode theory [30–33]. Defect modes in more complicated waveguides, as compared to a single square high index defect, have also been studied. In [34] the linear properties of a single low-index defect was studied in optically induced lattices. In [35] an optical lattice with a quadratic frequency modulation having a defect mode was investigated in the linear and the nonlinear regime. The transition from one-dimensional to two-dimensional lattices was realized using an optically induction technique [21,36] that let to the first experimental observation of two-dimensional discrete or lattice solitons [37]. This change in the dimensionality of the problem does not only modify the behavior of the system quantitatively but also qualitatively, resulting in a plethora of new phenomena that are not possible in one transverse dimension. For example, in two spatial dimensions, a bandgap can only exist if the depth of the periodic lattice exceeds a critical threshold [38] in contrast with the one-dimensional case [25, 26]. In addition, two-dimensional fundamental as well as gap lattice solitons have specific minimum power thresholds [38, 39]. Another family of solutions that is characteristic of the higher dimensionality is the vortex lattice soliton [39–41] which has been observed in photorefractive crystals [42, 43]. In two dimensions, the possibility for other types of lattices, such as Bessel [44], as well as building complex structures using solitons [45] opens up. For a review about recent experimental and theoretical results see [46].

It is interesting to notice that in all these works on waveguide arrays and optically induced lattices waveguiding is accomplished via TIR: If one waveguide of the lattice is isolated the resulting linear mode is guided due to the effect of TIR. Thus, the question that naturally arises is whether it is possible to make an array in which waveguiding is accomplished due to the presence of a photonic bandgap in the regions between the waveguides. And, furthermore, if such a lattice is possible, which are its fundamental linear and nonlinear properties and how do they differ from regular lattices.

In this paper, we propose a new type of waveguide lattice that relies on the effect of bandgap guidance, rather than TIR, in the regions between the waveguide defects. Two different general configurations of Bandgap Lattices (BGL), which are characterized by the defect refractive index are suggested. In these settings the refractive index of the defects is lower or higher compared to the average refractive index of the surrounding periodic structure. The differences between these “low index defect” and “high index defect” configurations are analyzed: First, in the linear regime, the bandgap and diffraction properties are examined and a simplified description of BGL based on CMT approximation is presented. The results obtained using this single band model [6], are in good agreement with the numerical simulations (in the regime where such an approximation is valid [26]). In the nonlinear case the Kerr effect can counteract diffraction leading to the formation of gap lattice solitons. Interestingly enough, in the case of low index defects, stable soliton solutions are localized in the low index areas independently of the intensity of light. This finding challenges the widely accepted idea that stable solitons can be sustained in high refractive index regions. We then vary the spacing between the defects to find that the coupling coefficient changes between positive and negative values.

#9692 - $15.00 USD Received 22 November 2005; revised 6 December 2005; accepted 6 December 2005

In the case of high index defects, the eigenvalue of the fundamental defect mode resides in the TIR regime. On the other hand, higher order modes exist inside the bandgaps. We analyze the second in order bandgap defect mode which exhibits a dipole structure. Notice that for this value of the defect spacing the coupling coefficient of this mode is negative. Physical settings where the linear and nonlinear properties of bandgap lattices can be experimentally realized are presented. These realizations can be arrays of waveguides, photonic crystal fiber arrays, and optically induced lattices. Similar configurations, consisting of a sequence of microcavities embedded in a photonic crystal, have been proposed in [12, 13]. In these latter cases however, and in two-dimensions, light is incident from a direction transverse to the microcavities or defects (and the resulting configuration is in the time domain). This is the fundamental difference from the proposed configurations, where light is axially excited and the propagation is in the space domain.

The basic differences between the work in hand and previous works on waveguide arrays and lattices are as follows: In square waveguide arrays strong (linear and nonlinear) localization is possible in the high index regions (or inside the waveguides). In a generic waveguide array, such localized modes can happen in the n lowest bands. The number of bands, n, where strong localization in the high index regions happens, depends on the depth and width of the single square well. The number of modes supported by a single waveguide is, in general, $m > n$. The first n waveguide modes decay fast enough so that one can apply CMT to the full periodic lattice. Notice that these m modes of the single waveguide structure are localized inside the defect due to the effect of TIR. As a direct result of CMT the n discrete eigenvalues will form the first n bands of the complete band structure. In this regime, linear modes (residing inside the bands) and nonlinear waves or solitons (residing either in the infinite bandgap or in the Bragg resonances or finite bandgaps) will be localized inside the high index regions. The higher bands (arising from radiation modes or from slowly decaying bound modes) are not strongly localized in either the high or the low index regions. Their amplitude has nodes and the intensity attains its maximum in the high or in the low index regions. Since these modes are not strongly localized, coupled mode theory can not be applied directly and a discrete nonlinear Schrödinger equation (DNLS) with nearest neighbor couplings can not be derived for such a model. Solitons can exist either in the finite or in the semi-infinite gaps of the resulting band structure. The solutions arising from the first n bands (where CMT can be applied) are going to be localized in the high index areas of the lattice. The rest of the families of gap soliton solutions represent extended solutions, and their maximum intensity at low total powers is not strongly localized either at the low or at the high refractive index areas. and an effective DNLS equation can not be derived. In the present work we propose that that by engineering the bandgap properties one can attain lattices whose Bloch modes are strongly localized in the low index regions. This happens due to the presence of a Bragg resonances between the defects. For example, if a single low index defect is isolated in this periodic structure this defect is going to be localized due to the effect of Bragg resonance rather than TIR [4, 11, 34, 47]. The presence of a periodic sequence of such defect is responsible for the formation of defect bands. As a result, and, most importantly, independently of the intensity of light, linear and nonlinear modes associated with this defect band can then strongly be localized in the low index regions, and CMT between low index defect modes can thus be directly applied.

2. Physical Settings

2.1. Low index guidance

Bandgap lattices rely on the phenomenon of Bragg resonance, rather than TIR, to confine light in the defect regions. Here, three basic physical settings where BGL can be experimentally observed are proposed:

#9692 - $15.00 USD Received 22 November 2005; revised 6 December 2005; accepted 6 December 2005

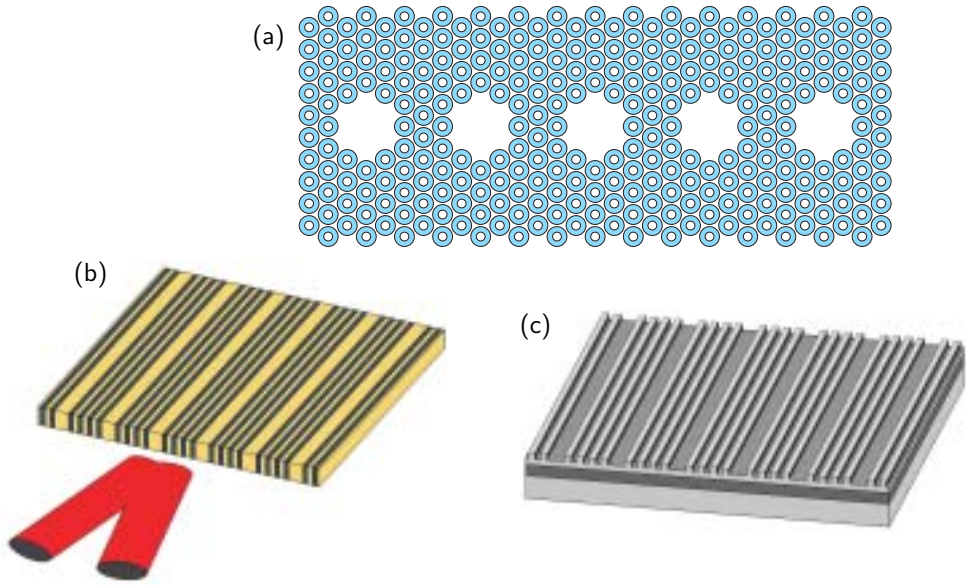

Fig. 1. Different physical settings where BGL can be implemented. These settings can be (a) photonic crystal fiber arrays, (b) optically induced lattices, and (c) waveguide arrays. Notice that higher index areas are shown in darker colors. In these configurations the intensity of light is expected to be localized in the *low* refractive index defects of the lattice.

The first one consists of a sequence of "Bragg reflection waveguides" [47–49]. A Bragg reflection waveguide is a one-dimensional bandgap structure designed to guide light at the low refractive index defect region. In the second transverse direction light is confined via TIR. By introducing a periodic sequence of low refractive index defects in the Bragg structure we can construct a Bragg reflection waveguide array [see Fig. 1(c)]. Such waveguides are experimentally feasible and can be implemented by etching the Bragg gratings and the defect regions [48, 50].

The second implementation is that of an array of PCFs [4, 5], such as the one shown in Fig. 1(a). The basic difference in this case is the requirement for the presence of a two-dimensional photonic bandgap in the $x-y$ plane. Again, the refractive index in the core of the PCFs is lower is compare than the average refractive index of the microstructure.

The third implementation is that of an optically induced lattice [21, 36]. By interfering pairs of plane-waves that play the role of Fourier components one should be able to reconstruct essentially any type of superlattice. The maximum number of plain waves that can be realized in an experiment is of course an additional constraint. Alternatively, this lattice can be partially coherent [51]. In such a lattice, the bandgap localization for a single low index defect has been demonstrated [34].

2.2. High index guidance

Waveguiding due to the presence of a photonic bandgap is also possible in the case of high refractive index defects, i.e., in the case where the refractive index of the defect is higher than the average refractive index of the lattice. In Fig. 2 a photonic crystal fiber array, an optically induced lattice, and a sequence of Bragg reflection waveguides, consisting of high refractive index defects are schematically presented. Later in this paper, it will be shown that there are

#9692 - $15.00 USD Received 22 November 2005; revised 6 December 2005; accepted 6 December 2005

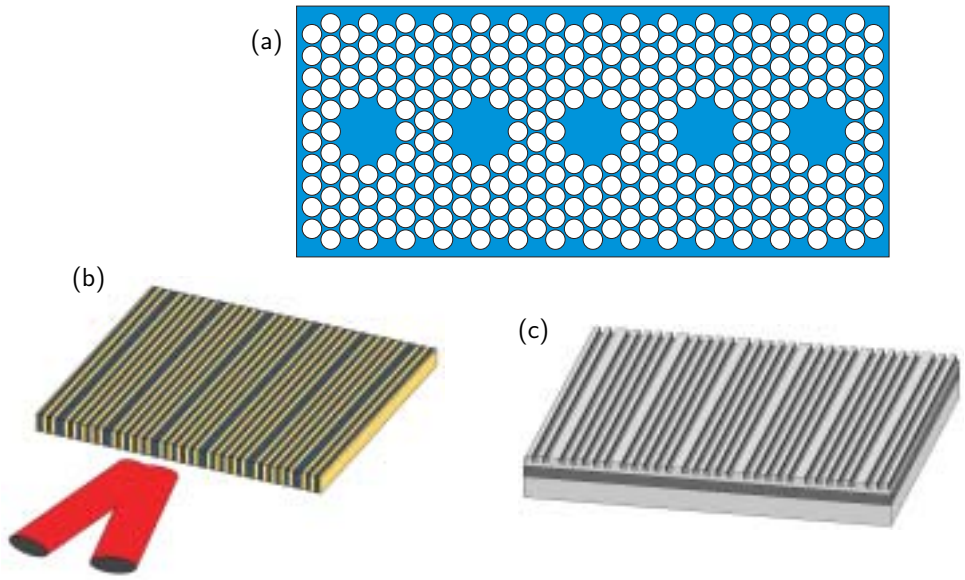

Fig. 2. Different physical settings where bandgap lattices can be implemented. These settings can be (a) photonic crystal fiber arrays, (b) an optically induced lattices, and (c) waveguide arrays. Notice that higher index areas are shown in darker colors. In these configurations the intensity of light is expected to be localized in the *high* refractive index defects of the lattice.

basic differences between these two types of bandgap waveguiding mechanisms, i.e., bandgap arrays with low or high refractive index defects.

2.3. Paraxial model 1

The mathematical modeling of the structures described previously is, in general, different in the three settings suggested. For example, nonlinear propagation in PCFs requires vectorial treatment. In biased photorefractive crystals the nonlinearity is of the saturable type. Here, we are going to use a generic approach that is based on the one-dimensional paraxial model

$$i\psi_z + \frac{1}{2}\psi_{xx} + V(x)\psi + \gamma|\psi|^2\psi = 0. \tag{1}$$

In Eq. (1) we assume that the medium is Kerr nonlinear (either focusing $\gamma = 1$ or defocusing $\gamma = -1$), and $V(x)$ is a potential proportional to the refractive index modulations of the array. On the other hand, propagation inside waveguide arrays is accurately described by Eq. (1). At relatively low power levels the saturable nonlinearity in photorefractives can be expanded in a Taylor series and a model similar to Eq. (1) can be obtained. In [52] an effective one-dimensional scalar model suitable for the description of two-dimensional photonic crystal fibers was derived.

By assuming that the propagation wavenumber of the electromagnetic wave is q,

$$\psi(x,z) = u(x)e^{iqz} \tag{2}$$

one can derive the corresponding eigenvalue problem

$$-qu + \frac{1}{2}u_{xx} + V(x)u + \gamma u^3 = 0. \tag{3}$$

#9692 - $15.00 USD Received 22 November 2005; revised 6 December 2005; accepted 6 December 2005

According to Bloch's theorem, the solutions of the linear eigenvalue problem can be written as

$$u(x) = g(x)\exp(ikx) \tag{4}$$

where $g(x) \equiv g(x;k) = g(x+L;k)$ and k is the corresponding "Bloch momentum". The potential in our problem consists of a periodic sequence of defects which are surrounded by periodic gratings. For convenience, and without loss of generality, we assume that the period of the this grating is equal to unity. Inside the primitive cell of the grating, which is defined in the domain $-1/2 < x \leq 1/2$, the potential is given by

$$V_g(x;V_0) = \begin{cases} V_0 & |x| < 1/4 \\ 0 & 1/4 < |x| \leq 1/2 \\ V_0/2 & |x| = 1/4 \end{cases} \tag{5}$$

where V_0 is the potential depth. Since the minimum of the potential is zero, V_0 provides the normalized index contrast of the structure. We can now express the potential for every spatial position x as

$$V_g(x) = V_g(x' = x - n) \tag{6}$$

where n is an integer and x' lies inside the primitive cell. The linear properties of this type of potentials were analyzed by Kronig and Penney [53]. Nonlinear Kronig-Penney models have also been considered in the literature [54–56].

It is worth mentioning that a general lattice of period L can be scaled to an equivalent lattice with period equal to unity. This can be readily shown by applying the transformation $x' = x/L$ along with $\psi' = \psi L$, $z' = z/L^2$ and $V_0' = L^2 V_0$. Evolution in the new scaled coordinates is now given by

$$i\psi_{z'}' + \frac{1}{2}\psi_{x'x'} + V(x';V_0')\psi' + \gamma|\psi'|^2\psi' = 0, \tag{7}$$

where the period in Eq. (7) is equal to unity.

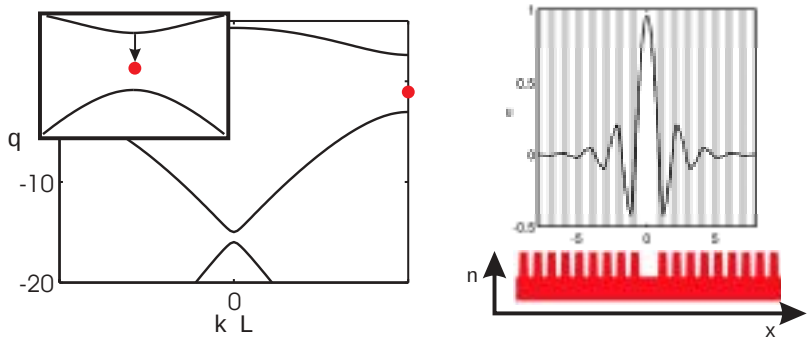

Fig. 3. On the left panel the band structure corresponding to the potential of Eq. (8) is shown. The period of this potential is $L = 1$ and its depth is $V_0 = 9$. The discrete spectrum is depicted with dots and the arrow indicates the band from which this mode bifurcates. The inset shows an enlarged view of the bifurcation. The first two bands of the spectrum have eigenvalues in the domains $[2.62\ 5.31]$ and $[-14.99\ -3.05]$, respectively. The eigenvalue of the first defect mode is $q = -1.59$. On the right panel the amplitude of the defect mode and a schematic illustration of the refractive index contrast across the lattice are shown.

#9692 - $15.00 USD Received 22 November 2005; revised 6 December 2005; accepted 6 December 2005

3. Low index guidance

3.1. Single defect

We assume that a defect is introduced at $x = 0$ inside this periodic lattice [as given by Eq. (5)]. The total potential is expressed as a sum of the periodic grating $V_g(x)$ minus the defect potential $V_d(x)$,

$$V_t(x) = V_t(x;V_0) = V_g(x;V_0) - V_d(x,V_0) \tag{8}$$

where

$$V_d(x;V_0) = \begin{cases} V_0 & |x| < 1/4 \\ V_0/2 & |x| = 1/4 \\ 0 & \text{otherwise} \end{cases} \tag{9}$$

The potential $V_t(x)$ is illustrated in Fig. 3. To understand the effect of the defect in the periodic lattice, let us first consider the linear paraxial model with a square potential (the potential is $V(x) = V_0$ inside the well and $V = 0$ outside the well). If the square well is absent the linear spectrum (diffraction relation) will extent to the region $q < 0$. By introducing a higher refractive index square well, we allow the presence of discrete eigenvalues in the spectrum which are "upshifted" (compared to the continuous spectrum) within the domain $0 < q < V_0$. Now, if the refractive index of the medium is that of Eq. (5) the spectrum consists of bands of finite extent. As a result of the presence of a lower refractive index defect inside this grating (8), discrete eigenvalues appear. Since the refractive index of the defect (9) is smaller than the average refractive index, we expect that the discrete spectrum (corresponding to the defect modes) will be "downshifted". This downshifting of the first defect mode can be seen in Fig. 3. On the left panel of Fig. 3 the eigenvalue of this defect mode bifurcating from the first (highest) band of the band structure is shown. This bifurcation can be illustrated by varying the defect strength, V_1, in Eq. (9) from 0 to V_0. When V_1 is small enough the eigenvalue of the defect mode is close to the first band, whereas, as V_1 increases the distance between the defect eigenvalue and the edge of the first band becomes larger. Since the mode in Fig. 3 has an eigenvalue in the first bandgap of the spectrum, it remains localized in the low refractive index region due to Bragg resonance. Notice that the mode shown in Fig. 3 is well localized inside the lattice. As it is known from solid state physics a bandgap defect mode decays exponentially. Thus, high localization of the latter requires a large exponential decay coefficient.

3.2. Bandgap lattice and coupled mode theory

We now consider a periodic sequence of defects inside a periodic lattice. The primitive cell of the resulting periodic refractive index structure is given by Eq. (8). The potential of this superlattice can be expressed as

$$V(x;V_0) = \begin{cases} V_g(x;V_0) - V_d(x,V_0) & |x| \le L/2 \\ V_g(x' = x - nL) - V_d(x' = x - nL) & |x| > L/2 \text{ and } |x'| \le L/2 \end{cases} \tag{10}$$

where L is the period and n is an integer such that x' is located inside the primitive cell. Here, we restrict ourselves to the specific case $L = 5$: This value is small enough to allow sufficient energy coupling among successive waveguides and big enough to render CMT to this problem. In the simulations the normalized refractive index contrast is $V_0 = 9$. A schematic illustration of the lattice is represented on the bottom of Fig. 4. Notice that the band structure has been computed using a plane wave expansion [57]: The linear problem is Fourier transformed and the resulting algebraic equations are solved numerically. In each case the window of our calculations is chosen to be equal to the period of the lattice. Furthermore, a single defect can be approximated by a periodic lattice with large period.

#9692 - $15.00 USD Received 22 November 2005; revised 6 December 2005; accepted 6 December 2005

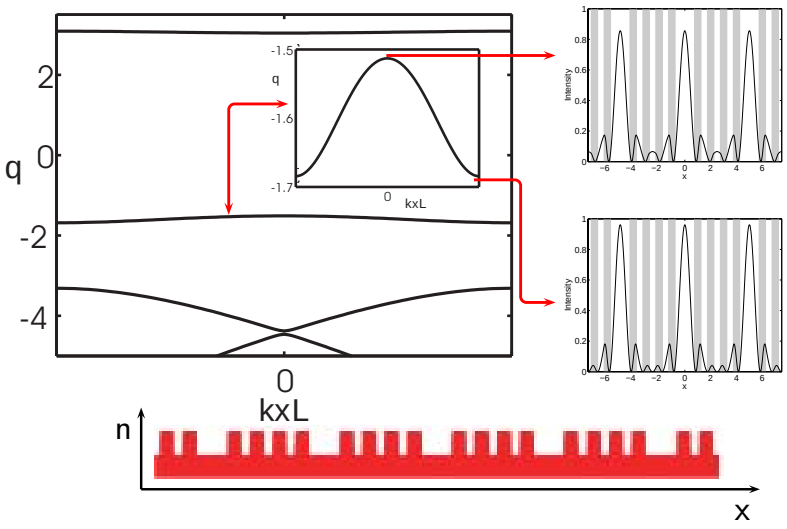

Fig. 4. The exact band structure (left panel) of a periodic superlattice as described by Eq. (10) for $V_0 = 9$ and $L = 5$. The inset shows an expanded view of the defect band. This band extends in the region $[-1.68 \ -1.51]$ while the bands above and bellow have spatial frequencies $[3.04 \ 3.09]$ and $[-4.38 \ -3.32]$, respectively. On the right panel the Bloch modes at the base and the edge of the Brillouin zone are depicted. On the bottom of the figure a schematic illustration of the refractive index modulation along the lattice is presented.

We are going to apply CMT to Eq (1). The first step is to consider the unperturbed linear eigenvalue problem of a single defect inside a periodic microstructure,

$$-q\phi + \frac{1}{2}\phi_{xx} + V_t(x)\phi = 0. \tag{11}$$

In Eq. (11) ϕ is the a localized defect mode with eigenvalue q, which lies deep inside a bandgap. The evolution of an optical wave propagating in a superlattice [that in our case is given by Eq. (10)] as a perturbation to Eq. (11) can now be considered. The main step in CMT consists of substituting the following expansion to Eq. (1) (which is considered as the perturbed problem)

$$\psi(x,z) = e^{-iqz}\sum_n c_n(z)\phi_n(x). \tag{12}$$

In this expansion $\phi_n(x) = \phi(x - nL)$ is a defect eigenmode of Eq. (11) localized at nL, and $c_n(z)$ incorporates the evolution of its amplitude along z. After some algebraic calculations the discrete nonlinear Schrödinger equation for the amplitudes of the localized modes is derived

$$i\frac{dc_n}{dz} + \Delta q c_n + \kappa(c_{n+1} + c_{n-1}) + \lambda|c_n|^2 c_n = 0 \tag{13}$$

where

$$\kappa = \frac{1}{2}\int_{-\infty}^{\infty}\phi_n^*\frac{d^2\phi_{n+1}}{dx^2}dx + \int_{-\infty}^{\infty}\phi_n^*\phi_{n+1}V(x)dx \tag{14}$$

is the of adjacent waveguide coupling strength,

$$\Delta q = \int_{-\infty}^{\infty}|\phi_n|^2(V(x) - V_t(x))dx \tag{15}$$

#9692 - $15.00 USD Received 22 November 2005; revised 6 December 2005; accepted 6 December 2005

is a shift in the spatial frequency of the eigenmodes, and

$$\lambda = \gamma \int_{-\infty}^{\infty} |\phi_n|^4 dx \tag{16}$$

is the Kerr nonlinear coefficient. The diffraction relationship can be found by substituting in the linear part of Eq. (13) the plane wave solution $c_n = \exp(iqn - ikx)$. The resulting diffraction relation satisfies the condition

$$q = \Delta q + 2\kappa \cos k. \tag{17}$$

In addition, we have computed the exact band structure of the superlattice (10) which is shown in Fig. 4. The coupling coefficient can be calculated using different methods. The first is straightforward; it requires the computation of the defect modes and the direct evaluation of the overlap integrals in Eq. (14). Alternatively, in this case it is simpler to match the width of the exact defect band diffraction relation, with 4κ. The resulting coupling coefficient was found to be $\kappa = 0.0857$. The shift Δq can also be computed indirectly. It is equal to the difference between the average value of q in the superlattice band structure and the eigenvalue of the defect mode. According to our calculations this shift is negative and equal to $\Delta q = -0.006$. Notice that the sign of Δq in Eq. (15) depends on the sign of perturbation in the potential $V(x) - V_t(x)$. In the specific lattice of Eq. (10) this difference is always negative. Thus, the shifting of the band structure, Δq, is also negative. This is a general feature for low index defect guidance. In contrast, if the defects are high index, the integral in Eq. (15) is positive and so is Δq.

In Fig. 4 we can also see the Bloch modes (normalized to unity) corresponding to the base and the edge of the Brillouin zone. These modes have similar profile. The main difference between the modes at the base and the edge of the Brillouin zone is that the latter one has an additional node (the field becomes zero) at the edge of the primitive cell of the lattice.

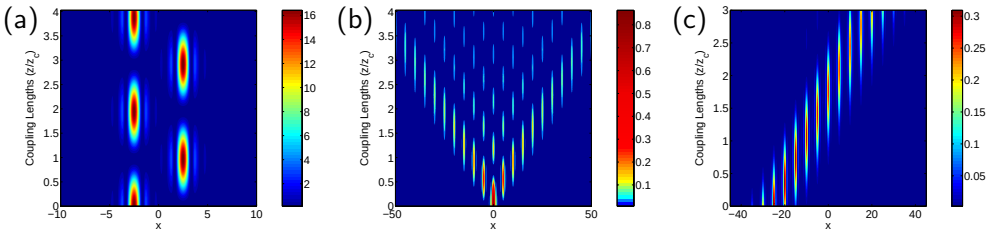

Fig. 5. Numerical simulations of low power (linear) beams propagating according to Eq. (1) where the lattice is given by Eq. (10). In (a) only two defects are involved, thus, forming a directional bandgap coupler, (b) diffraction of a single waveguide excitation, and (c) propagation with minimum diffraction when the beam is launched with a Bloch momentum $k = \pi/2L$ that corresponds to the middle of the Brillouin zone. (a) and (b) the initial condition is the localized mode of a single low index defect and in (c) it is a Gaussian superposition of single defect modes having the proper phase difference. The propagation length is normalized to the coupling length $z_c = \pi/\kappa$. Because the maximum beam intensity reduces rapidly as it diffracts, a highly nonlinear scheme in the color range (b) able to capture the diffraction pattern for several diffraction lengths is utilized.

We have performed direct numerical simulations using the paraxial model of Eq. (1) where the potential is given by Eq. (10). Our goals are to study the linear properties of the lattice and to test the validity of the results derived from the CMT. The numerical results are presented in Fig. 5. In Fig. 5(a) two defects are involved which form a bandgap coupler. Notice that in CMT (13) a coupler is described by two equations for the amplitudes c_0 and c_1. It is known that

#9692 - $15.00 USD Received 22 November 2005; revised 6 December 2005; accepted 6 December 2005

if the beam is originally launched in one waveguide, the energy is completely transfered to the other waveguide at $z_c = \pi/\kappa$, where z_c is the coupling length. From the numerical simulations is found that $z_c = 37$, which corresponds to a coupling coefficient $\kappa = 0.0849$. This value is in excellent agreement with the coupling coefficient as obtained from the band structure calculations. Notice that in all of the simulations shown in Fig. 5 the power propagates via coupling between low index regions. The in between Bragg gratings are the intermediate tunneling areas (via exponentially decaying waves).

A characteristic feature of the discrete model (13) is the low power ($\lambda = 0$) diffraction pattern when only one lattice site is excited, i.e., $c_n(z=0) = \delta_{n,0}$. This pattern is expressed in terms of Bessel functions

$$c_n(z) = J_n(2\kappa z)\exp(i\pi n/2 + i\Delta q z) \tag{18}$$

and for relatively large z its maximum intensity $|c_n(z)|^2$ is not located on the central waveguide but, instead, on the two side lobes. The diffraction pattern as found, by solving Eq. (1) with the lattice of Eq. (10), when only one waveguide is excited is shown in Fig. 5(b) and is in very good agreement with Eq. (18).

Subsequently, the waveguide lattice is excited with a relatively broad Gaussian beam having the form

$$\psi(x, z=0) = \sum_n \phi_n(x) e^{-(n/A)^2} e^{ikn}, \tag{19}$$

where $A = \sqrt{5}$ and the Bloch momentum is located exactly in the middle of the Brillouin zone, i.e., $k = \pi/2L$. For this value of k the second order diffraction is zero and the beam is expected to broaden due to asymmetric third order and symmetric forth order diffraction [58]. Utilizing CMT, the group velocity of the beam is found to be $v_g = 2\kappa$. As expected, when the initial condition is given by Eq. (19), the beam propagates with relatively small broadening for over four diffraction lengths [see Fig. 5(c)].

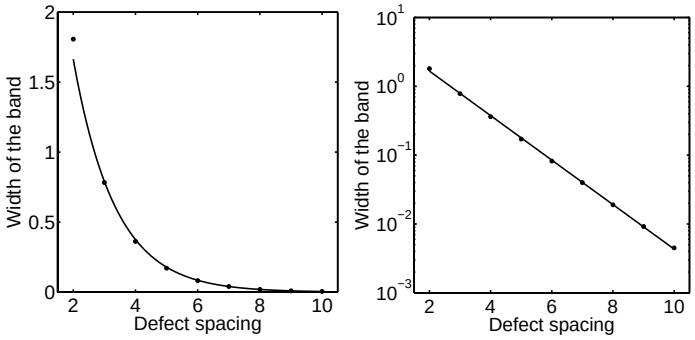

Fig. 6. On the left panel we can see the dependence of the width of the defect band from the spacing between the defects. On the right panel we plot the same data in a logarithmic scale for the width of the defect band. The data are presented with dots and the solid curve show the fitting function.

We are now going to study how the band structure properties change when the spacing between two successive defects is varied. This can be accomplished by changing the period L of the waveguide structure in Eq. (10). Notice that the requirement for a regular periodic surrounding grating limits the allowed values for L to the discrete range $L = n$, where n is an integer grater or equal to 2. The case where L is between 2 to 10 is examined. In general, as the spacing between the defects increases the width of the band decreases (and as a result the same happens to the coupling κ between adjacent defects). In Fig. 6 we plot the width of the

#9692 - $15.00 USD Received 22 November 2005; revised 6 December 2005; accepted 6 December 2005

defect band as a function of the defect spacing in both linear and logarithmic scales. As one can see, the data in the logarithmic scale are very close to a straight line. Thus, the width of the defect band should decay exponentially with the spacing. Utilizing a least square curve fitting of the numerical data to the function $W = a\exp(-bL)$ we found that the optimum values are $a = 7.376$ and $b = 0.7443$. It is worth mentioning that the exponential decay in the defect band width can be predicted from CMT, since the integrals in Eq.(14) incorporate exponentially decaying functions. Notice that the first point corresponding to defect spacing 2 does not fit well with the exponential curve. We render this deviation from the exponential rule to the fact that if two adjacent defects are close enough to each other CMT can not be applied, as a result, the same holds true for the exponential decay in the coupling strength. The bandgaps above and below this defect band are also affected by the period L. More specifically, we noticed that as the spacing between the defects increases the bandgaps above and below the defect band also increase.

Another interesting property is that not only the magnitude but also the sign of the coupling strength κ changes with the defect spacing. More specifically, when the period is an odd number ($L = 3,5,7,9,\ldots$) the coupling between adjacent defects is positive. On the other hand, when the period of the bandgap lattice is an even number ($L = 2,4,6,8,10,\ldots$) the coupling strength is negative. One can comprehend this behavior by noticing that the derivative of the original parabolic dispersion relation, dq/dk, of a uniform index medium is maintained when periodic index modulations are introduced (in the extended zone scheme). As a result, in the reduced zone scheme, different periods can correspond to different signs of the coupling strength. This effect can modify the properties of lattice solitons that are associated with the defect band. Specifically, in regular lattices with positive coupling coefficients ($\kappa > 0$), self-focusing nonlinearities result to in-phase soliton solutions. These solitons reside at the base of the Brillouin zone, and the phase difference of the field among adjacent waveguides is a multiple of 2π. In contrast, in the case of self-defocusing nonlinearities the soliton solutions reside at the edge of the Brillouin zone and are π-out-of-phase (i.e., the phase difference among successive waveguides is equal to $2n\pi + \pi$, n being an integer). Due to the presence of negative coupling ($\kappa < 0$) we expect that this behavior will be inverted: self-focusing solitons will be π-out-of-phase and self-defocusing solitons will be in-phase. This becomes apparent by noticing that Eq. (13) is invariant under the transformation $\kappa \to -\kappa$, $\lambda \to -\lambda$, $z \to -z$, $c_n \to c_n \exp(i2\Delta qz)$. Notice that negative coupling coefficients are also possible in photonic crystals [12, 13, 59].

3.3. Low index solitons

Before proceeding any further in the analysis of solitons in bandgap lattices, we would like to mention that there exist two quantities which are conserved by Eq. (1), namely the total power of the beam

$$P = \int_{-\infty}^{\infty} |\psi|^2 dx, \tag{20}$$

and the Hamiltonian

$$H = \int_{-\infty}^{\infty} \left[\left| \frac{\partial \psi}{\partial x} \right|^2 - 2V(x)|\psi|^2 - |\psi|^4 \right]. \tag{21}$$

These quantities can be exploited in the analysis of solitons properties. As we will see, the effect of nonlinearity in Eq. (1) with a lattice given by (10) can counteract diffraction resulting to the formation of self-localized beams or lattice solitons. Assuming that the soliton solution has the form of Eq. (2), i.e.,

$$\psi(x,z) = u(x)\exp(iqz)$$

the nonlinear eigenvalue problem of Eq. (3) is derived. This latter Equation can be solved numerically using, for example, the Newton's iteration method.

#9692 - $15.00 USD Received 22 November 2005; revised 6 December 2005; accepted 6 December 2005

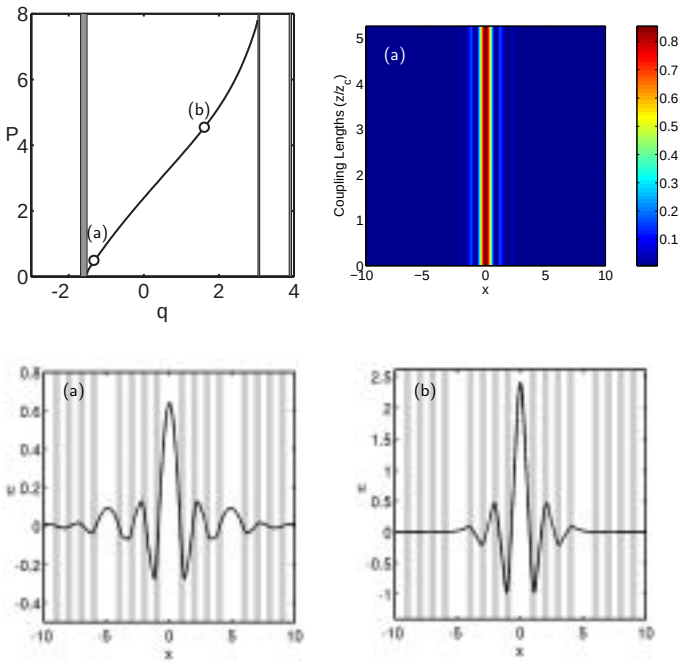

Fig. 7. Self-focusing soliton solutions of the low index defect lattice given by Eq. (10) with period $L = 5$ and index contrast $V_0 = 9$. In the top left panel the existence curve of this family of soliton solutions (total power vs. the eigenvalue) is presented. The bandgaps are shown in gray color and the bands in white. The two defect modes corresponding to points (a) and (b) of the existence curve, with eigenvalues $q = -1.33$ and $q = 1.61$ respectively, are depicted in the bottom panel. The stable evolution of mode (a) over 5 diffraction lengths is presented in the top right panel.

Let us first analyze the formation of bandgap solitons in self-focusing lattices i.e., $\gamma = 1$. The existence curve of such a family of soliton solutions in a lattice given by Eq. (10) is shown on the upper left panel of Fig. 7. The total power P of the soliton as a function of its eigenvalue q is plotted. The existence curve is lying in the bandgap between two bands. The band located on the left of the existence curve is the defect band. These bands are quite thin compared to the bandgap region. We notice that on the left side of the existence curve the total soliton power goes to zero, whereas on the right side the total power approaches a constant maximum value. This can be explained by the fact that the effective diffraction of the band close to the left part of the existence curve is normal and, thus, compatible to the self-focusing nonlinearity. As a result, a soliton can be formed even for a very small value of the nonlinearity as it is expected for one-dimensional lattices. This can be shown mathematically, by taking values of q close to the band edge and employing the Bloch envelope approximation [60], from which an effective nonlinear Schrödinger (NLS) equation is derived. It is known that the total power of the fundamental NLS soliton goes to zero as q approaches the band edge. On the other hand, the effective diffraction close to the right part of the existence curve is anomalous and, thus, incompatible with the self-focusing nonlinearity. In this case a high intensity defect is responsible for the soliton trapping. This family of solutions has a maximum power threshold. The two specific examples depicted as circles on this curve [(a) and (b)], corresponding to eigenvalues $q = -1.33$ and $q = -1.61$, respectively, are presented on the bottom of the figure. We examined the stability

#9692 - $15.00 USD Received 22 November 2005; revised 6 December 2005; accepted 6 December 2005

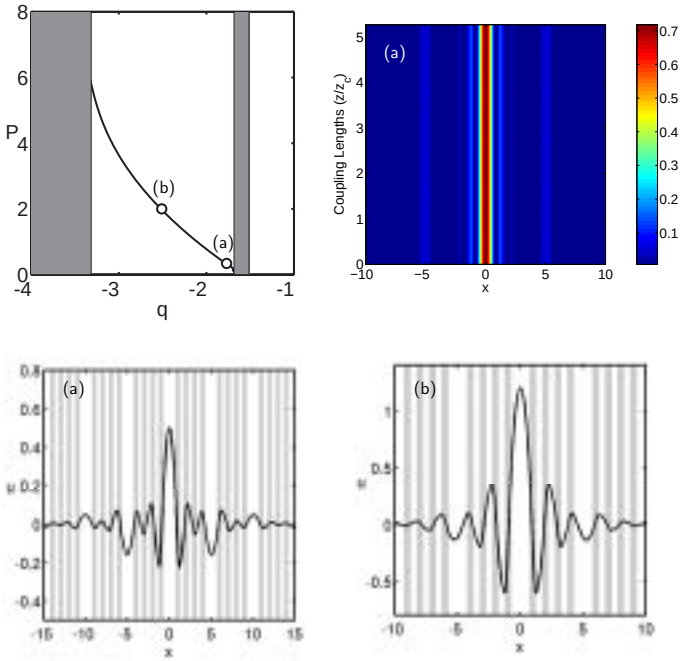

Fig. 8. Self-defocusing soliton solutions of the low index defect lattice given by Eq. (10) with period $L = 5$ and index contrast $V_0 = 9$. In the top left panel the existence curve of this family of soliton solution (total power vs. the eigenvalue) is presented. The bandgaps are show in gray color and the bands in white. The two defect mode corresponding to points (a) and (b) of the existence curve, and with eigenvalues $q = 1.77$ and $q = -2.51$ respectively, are depicted in the bottom panel. The stable evolution of mode (a) over 5 diffraction lengths is presented in the top right panel.

of these solitons numerically by performing direct numerical simulations. As initial conditions the numerically found soliton solutions with superimposed random perturbations are used. The random noise guarantees that all the linear eigenmodes of the perturbed problem will be excited and instability will develop fast. The soliton solutions are found to be stable in most of the cases considered. For example, on the top right panel of Fig 7 one can see the stable evolution of the soliton mode (a). As it can be see at the bottom of Fig. 7 (where the high index regions are gray areas) the maximum intensity of these solitons is located in the low refractive index regions of the medium. For this reason we call this family of solutions *low index solitons*.

Low index solitons also exist in self-defocusing media ($\gamma = -1$). In Fig. 8 we can see the existence curve and specific examples of soliton solutions when the nonlinearity is self-defocusing. This family of solitons resides in the bandgap which is located on the left side of the defect band (whereas soliton with focusing nonlinearity exist on the bandgap which is located on the right side of the defect band). A basic difference from their self-focusing "cousins", is that the total power of self-defocusing bandgap solitons approaches to zero on the right side of the existence curve. To understand this behavior, we stress the fact that the effective diffraction at the edge of the defect band, which is close to point (a) in the existence curve, is anomalous and, thus, compatible with self-defocusing nonlinearity. One can apply the Bloch envelope approximation to show that the total power goes to zero as the eigenvalue approaches the band edge. On the other side of the existence curve the total power of these low index solitons approaches a maximum

#9692 - $15.00 USD Received 22 November 2005; revised 6 December 2005; accepted 6 December 2005

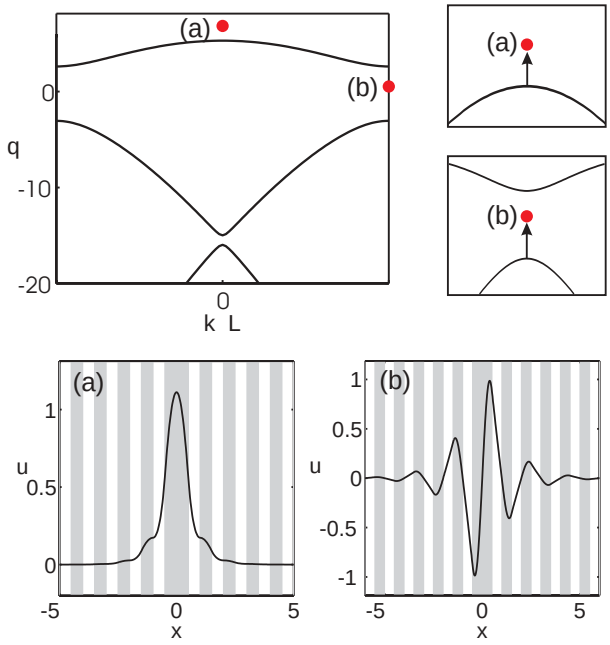

Fig. 9. On the top left panel the band structure corresponding to the potential which is expressed by Eq. (22) is shown. The continuous part of the spectrum (the bands) of this potential is exactly the same as that of Eq. (10) (shown in Fig. 4). The period of this potential outside the defect is $L = 1$ and its depth is $V_0 = 9$. The first two modes of the discrete spectrum (which are associated with the defect) are depicted with dots, and the arrows indicate the bifurcations of these modes from the continuous bands. The top right panel shows enlarged views of these bifurcations. On the bottom panel the first two defect modes [(a) and (b)] are shown. The first two bands of the spectrum have eigenvalues in the regions $[2.62\ 5.31]$ and $[-14.99\ -3.05]$, respectively. The eigenvalue of the first defect mode (located in the TIR region) is $q = 6.84$ and of the second mode (located in the first bandgap between the first two bands) is $q = 0.53$.

value, which determines a specific power threshold. The field profiles of two different solitons corresponding to points (a) and (b) on the existence curve are shown on the bottom panel of Fig. 8. The stable evolution of mode (a) is shown on the top right panel of the same Figure.

We would like to mention that for this specific value of the spacing the coupling κ is positive. As a result self-focusing solitons are expected to be in-phase and the self-defocusing solitons are expected to be π-out-of-phase. As explained before, the opposite is also possible: For example, the coupling can become negative if the normalized adjacent waveguide spacing is 4 or 6. As a result of the negative coupling, the self-focusing solitons are π-out-of-phase and the self-defocusing solitons are in-phase. Notice that the presence of a sequence of defects allows for strong localization of solitons in the low-index regions independently of the total soliton power.

4. High refractive index guidance

Waveguiding inside the bandgap is also possible when the defect has high index. Let us first consider a single high index defect inside the periodic lattice. The defect we are going to use

#9692 - $15.00 USD Received 22 November 2005; revised 6 December 2005; accepted 6 December 2005

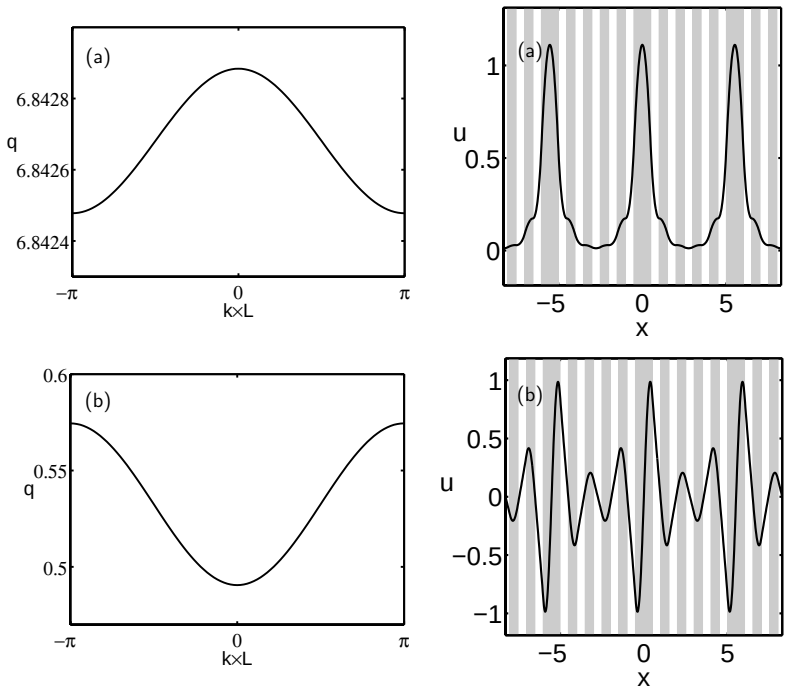

Fig. 10. Expanded view of the first two defect bands [(a) and (b)] inside the band structure (left panel) of a periodic superlattice as described by Eq. (23) for $V_0 = 9$ and $L = 5.5$. Bands (a) and (b) originate from the corresponding defect modes of Fig. 9. The narrow defect band (a) spans the region [6.8425 6.8429] while the band bellow has spatial frequencies in the domain [5.11 5.16]. Defect band (b) spans the region [0.49 0.57] while the bands above and bellow have spatial frequencies in the domains [3 3.16] and $[-3.35\ -4]$, respectively. On the right panel the Bloch modes of bands (a) and (b) at the base of the Brillouin zone are shown.

has the form

$$V_t(x) = V_t(x;V_0) = V_g(|x| - 1/4) \tag{22}$$

where $V_g(x)$ is given by Eqs. (5)-(6). Using arguments similar to those presented in the previous section, we expect that localized modes, which bifurcate from band edges, will then emerge (Fig. 9). More specifically, a discrete eigenvalue will bifurcate from the base of the first Brillouin zone towards the total internal reflection region. In Fig. 9 this is shown as mode (a). This mode remains localized inside the defect due to TIR. Qualitatively, we can understand that in this case guidance relies on the average refractive index of the medium; the refractive index of the defect is higher than the average index of the surrounding grating. Notice, that the amplitude of the TIR defect does not have any nodes (the field does not become zero along x).

An additional bifurcation occurs at the edge of the second Brillouin zone, giving rise to a higher order defect mode with an eigenvalue lying between the first and the second band. This mode [mode (b) in Fig. 9] stays localized due to the effect of Bragg resonance (or photonic bandgap). Inside the defect region the profile of this mode is dipole-like: the field is zero at the center of the defect and positive (negative) for small positive (negative) displacements in x.

We now introduce a sequence of such high index defects inside the periodic lattice. The

#9692 - $15.00 USD Received 22 November 2005; revised 6 December 2005; accepted 6 December 2005

resulting periodic potential or superlattice is given by

$$V(x) = V(x;V_0) = V_t(x' = x - Ln;V_0), \tag{23}$$

where L is the period of the superlattice, n is an integer such that $-L/2 < x' \leq L/2$ and $V_t(x)$ is given by Eq. (22). The presence of a sequence of defects that are close to each other breaks the eigenvalue (spatial frequency) degeneracy and the defect eigenvalues form bands. We have computed the resulting band structure in the specific case $V_0 = 9$ and $L = 5.5$ witch is presented in Fig. 10. Since the defect mode (a) residing in the TIR region is highly confined, the overlap between successive defect modes is small and the resulting band structure is narrow. The coupling coefficient for this band is found to be $\kappa = 10^{-4}$. On the other hand, it is quite interesting to notice that the defect band (b), created inside the bandgap, is "inverted" compared to the defect band (a). That is, the spatial frequencies at the edge of the Brillouin zone are higher compared to those at the base of the Brillouin zone. As a result, the coupling coefficient is going to be negative $\kappa = -0.021$.

Finally, numerical simulations similar to those presented in Fig. 5 have been performed in order to confirm the linear behavior as compared to CMT. The numerical simulations are in very good agreement with the CMT predictions. It is worth mentioning that in the case of photonic crystal fibers, and according to the photonic structure of the lattice, the eigenmodes can become degenerate: For example, in two-dimensions dipole modes oriented along two different directions can have the same eigenvalue, depending on the structure of the surrounding crystal.

5. Conclusions

In conclusion, we proposed a new type of waveguide lattice that relies on the effect of bandgap guidance, rather than total internal reflection, in the regions between the waveguide defects. Two different setting, corresponding to low index and high index defects were suggested. We analyzed the linear bandgap and diffraction properties of such lattices. We showed that in the nonlinear regime the Kerr effect can counteract diffraction leading to the formation of gap lattice solitons. Interestingly enough, in the case of low index defects, stable soliton solutions are localized in the low index regions. This finding challenges the widely accepted idea that stable solitons can be sustained in high refractive index regions. In addition, in the case of high index defects, the coupling coefficient can become negative. Physical realizations where the linear and nonlinear properties of bandgap lattices can be experimentally verified were presented. Let us mention before closing that the properties of nonlinear waves in high index defects have not been considered in this work. In a subsequent work it would be interested to study, for example, nonlinear twisted modes and study their stability in focusing and defocusing media.

Acknowledgments

This project is co-funded by the European Social Fund (75%) and National Resources (25%)-Operational Program for Educational and Vocational Training II (EPEAEK II) and particularly the Program PYTHAGORAS.

#9692 - $15.00 USD Received 22 November 2005; revised 6 December 2005; accepted 6 December 2005